©2002 The Visualization Society of Japan and Ohmsha, Ltd.
Journal of Visualization, Vol. 5, No. 3 (2002) 243-254

Development of Genetic Algorithm Based 3D-PTV Technique

Doh, D. H.*1, Kim, D. H.*1, Cho, K. R.*1, Cho, Y. B.*1, Lee, W. J.*1, Saga, T.*2 and Kobayashi, T.*2

*1 Division of Mechanical and Information Engineering, Korea Maritime University, Youngdo-ku, Dongsam-dong, Busan 606-791, Korea.
*2 Institute of Industrial Science, The University of Tokyo, 4-6-1 Komaba, Meguro-ku, Tokyo 153-8505, Japan.

Received 8 December 2001.
Revised 25 March 2002.

***Abstract*:** A new 3D-PTV technique has been developed using GA (Genetic Algorithm). The measurement system consists of three CCD cameras, Ar-ion laser, an image grabber and a host computer. One-to-one correspondences are made by taking advantage of the combinatorial optimization of the genetic algorithm for the whole particles of the two images during the time interval of image frames. Two fitness functions are introduced in order to enhance the correspondences of the particles. One is based on the concept of continuum theory and the other one is based on the minimum error of three-dimensional distance. Performance of the developed algorithm is tested using a set of virtual images constructed by the use of LES data set on an impinging jet. The developed 3D-PTV system is successfully applied to the measurement of flow characteristics of the wake of a circular cylinder.

***Keywords*:** 3D-PTV, genetic algorithm, impinging jet, circular cylinder.

1. Introduction

There have been many algorithms in Particle Image Velocimetry (PIV) and Particle Tracking Velocimetry (PTV) (Adrian, 1991). Cross-correlation method (Utami and Blackwelder, 1991) and four-step particle tracking method (Kobayashi et al., 1991) were properly used for each purpose. Regardless of the method chosen, it was desirable to measure three-dimensional instantaneous structures of flows with high resolutions. 3D-PTV has better benefits than 3D-PIV as it can be extended to three-dimensional volume measurements.

Yamada and Yamane (1995) and Ohyama et al. (1993) adopted the genetic algorithm (Goldberg, 1985) to PTV in order to increase the number of vectors to be obtained. They defined a fitness function in which the displacement of each pair of particles was assumed to have a minimum value. They applied their GA (Genetic Algorithm)-PTV algorithm to the measurement of a forced vortex and obtained about 80% of correct vectors from initial velocity vectors. Doh et al. (2000a) could obtain more than 98% of correct vectors from initial velocity vectors for the same flow field using virtual images by introducing a modified GA algorithm in which a concept of migration was used as the GA operator.

In the meantime, there had been many attempts to increase the number of instantaneous three-dimensional vector distribution with 3D (three-dimensional)-PTVs in order to probe the flow structures (Kasagi et al., 1987; Racca and Dewey, 1988; Kobayashi et al., 1989) since Chang and Tatterson (1983) had firstly constructed a practical 3D-PTV based on the stereo photogrammetry. Kasagi and Nishino (1991) obtained about 400 instantaneous vectors near the boundary layer of a wall and showed their results were in good agreements with other results though instantaneous structures could not be captured. Maas et al. (1993) were able to get about 1000 instantaneous three-dimensional velocity vectors for three-dimensional channel flow. Doh et al. (2000b) obtained

about 500 instantaneous three-dimensional velocity vectors for a relatively complex flow field, the wake of a backward-facing step, by applying a match probability concept (Ballard and Brown, 1982) in pairing the particles of the two different images. Most of the previous results failed in showing the instantaneous physical properties of the flow field.

In this study, a new 3D-PTV system that can measure instantaneous three-dimensional physical properties of complex flows is proposed by adapting a modified type of that algorithm suggested by Doh et al. (2000a). The measurement system could obtain about 2000 to 3000 instantaneous three-dimensional velocity vectors for relatively complex flow fields with low-resolution cameras (512 × 512 pixels). The number of correct vectors obtained in one processing was about 75% of the number of particles, which is quite promising for the constructed system to be able to directly probe the flow structure itself for any complex flow if high-definition cameras are used. The wake of a circular cylinder was measured by the constructed GA-3D-PTV system, and a validation was made on the constructed system through a comparison with the results obtained by other methods.

2. GA-based 3D-PTV System

In order to obtain three-dimensional velocity vectors, parameters of each camera, such as position of viewing point, tilting angles, focal length, distortion coefficients of camera lens and deviation between the viewing point and the center of CCD cell should be known in advance. Next, three-dimensional positions of each particle should be calculated based on the parameters of cameras. Finally, three-dimensional displacements of each particle can be obtained using the GA algorithm proposed in this study. Three-dimensional velocity of each particle is then obtained just by dividing the displacement by the time interval of image frames.

2.1 Calculation of Camera Parameters and Three-dimensional Positions of Particles

The calibration of camera was made using a calibrator. 42 landmarks were installed on the calibrator. The landmarks were arranged three-dimensionally on a table (80 × 110 × 10 mm). Small machined spheres of 1 mm diameter were located at the tip of 0.5 mm diameter poles and they were painted in white. The centers of all small spheres and their relative positions were measured with an optical instrument with 1/1000 mm precision. The absolute coordinates and their photographic coordinates were used to calculate the parameters of cameras.

In this study, 10 parameters (6 exterior parameters: *dis*, a, b, g, m_x, m_y, 4 interior parameters: c_x, c_y, k_1, k_2) were obtained. (a, b, g) represents the tilting angles of the axes of the photographic coordinates against the absolute axes. Figure 1 shows a coordinate relation when the photographical axes had been set to parallel with the absolute coordinate by tilting with the angles (a, b, g). (X, Y, Z) represents the absolute coordinate, and (x, y, z) the photographical coordinate of the objective point. The notation *dis* means the distance between the origin O (0, 0, 0) and the principal point (X_0, Y_0, Z_0) of the camera.

The coordinate (X_m, Y_m, Z_m) represents the position of the point P when the camera coordinate is rotated with the tilting angles to make the collinear set in one line as shown in Fig. 1. The m_x, m_y means the point at which the normal vector from the origin O(0, 0, 0) of the camera coordinate meets with the X-Y plane. The collinear equation

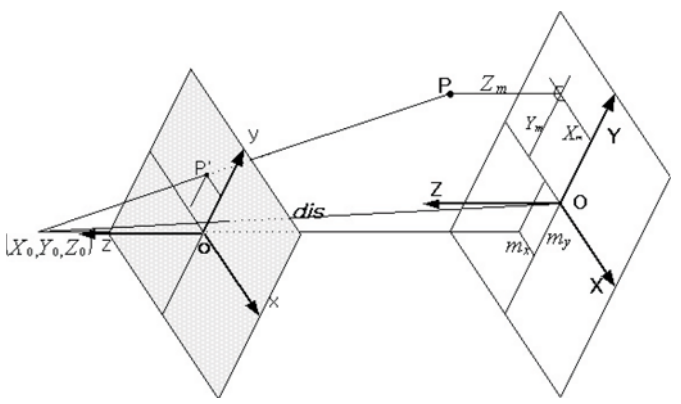

Fig. 1. Camera parameters and their relations between the absolute coordinate and the photographical coordinate.

for every point between the two coordinates is expressed as Eq. (1). c_x and c_y are the focal distances for x and y components of the coordinate. Dx and Dy are the lens distortions as expressed as Eq. (2). An improved Gauss-Newton calculation method (Doh, 1995) was adopted to obtain all necessary parameters of camera using the above two equations. The three-dimensional position of particles was regarded as an intersection of corresponding perspective rays of the two cameras. The collinear equation for each camera can be given as Eq. (3).

$$x = c_x \frac{Y_m - m_x}{\sqrt{dis^2 - m_x^2 - m_y^2} - Z_m} + Dx \qquad y = c_y \frac{Y_m - m_y}{\sqrt{dis^2 - m_x^2 - m_y^2} - Z_m} + Dy \tag{1}$$

$$Dx = (x/r) \times (k_1 r^2 + k_2 r^4) \qquad Dy = (x/r) \times (k_1 r^2 + k_2 r^4)$$
$$r = \sqrt{x^2 + y^2} \tag{2}$$

$$\begin{pmatrix} X \\ Y \\ Z \end{pmatrix} = \begin{pmatrix} a_{11} & a_{12} & a_{13} \\ a_{21} & a_{22} & a_{23} \\ a_{31} & a_{32} & a_{33} \end{pmatrix} \begin{pmatrix} x \\ y \\ -c \end{pmatrix} + \begin{pmatrix} X - X_o \\ Y - Y_o \\ Z - Z_o \end{pmatrix} \tag{3}$$

The absolute coordinates, X, Y and Z were transformed from the image coordinates, x and y. c is composed of c_x and c_y. The elements of the rotation matrix a_{ij} were obtained from camera calibration. Three cameras (A, B, C) were used and each two-camera set, (A, B) and (A, C), contributed to produce the final three-dimensional velocity vectors. Since the corresponding perspective rays of the two cameras do not intersect at one point due to uncertainties associated not only with the uncertainty of the landmarks but also with the photographical coordinates of particle image, a least square method was adopted in obtaining the coordinate (X, Y, Z) in Eq. (3). The three-dimensional positions of every particle can be expressed as Eq. (4) for the two sets of cameras (A, B) and (A, C).

$$\begin{bmatrix} X_P \\ Y_P \\ Z_P \end{bmatrix} = \frac{1}{2} \left\{ \begin{bmatrix} X_A \\ Y_A \\ Z_A \end{bmatrix} + \begin{bmatrix} X_{BorC} \\ Y_{BorC} \\ Z_{BorC} \end{bmatrix} \right\} \tag{4}$$

Here, X_A, Y_A and Z_A represent the absolute coordinates for camera A defined in Eq. (3). $X_{B\,or\,C}$, $Y_{B\,or\,C}$ and $Z_{B\,or\,C}$ are for camera B or C. Since the three-dimensional positions defined by these coordinates theoretically are sometimes not identical, mean value as defined in Eq. (4) is considered as the final three-dimensional position of particle.

In order to calculate the three-dimensional positions of particles, corresponding pairs of particles in the two sets of camera images should be obtained among many other particles. In order to find corresponding pairs, a genetic algorithm coupled with 3D-PTV algorithm has been used. The detail to find the corresponding pairs is described below.

2.2 Genetic Algorithm based 3D-PTV Algorithm

A genetic algorithm was adopted to increase the number of true pairs among many possible pairs of particles in each pair of camera image. Table 1 shows the definition of chromosome used in PTV. Figure 2 shows the calculation procedure of the genetic algorithm. Four major GA operators such as isolation, reproduction, crossover and migration were used. A chromosome consists of two photographic coordinates of two sets of cameras. The initial population was generated through a calculation process in which bad pairs were separated from a selected group into an unselected group by using a threshold value $3DE$, expressed as a fitness function in Eq. (5).

$$3DE = (D_o + D_t)/2 \tag{5}$$

where,

$$D_{o.\,or\,.t} = \sqrt{(X_{B.\,or\,.C} - X_A)^2 + (Y_{B.\,or\,.C} - Y_A)^2 + (Z_{B.\,or\,.C} - Z_A)^2}$$

D_o: distance of the two three-dimensional positions of vector original points
D_t: distance of the two three-dimensional positions of vector terminal points
X_A, Y_A, Z_A, X_B, Y_B, Z_B, X_C, Y_C, Z_C: three-dimensional position of particle defined by each camera

Table 1. Definition of chromosome with respect to two sets of cameras.

Camera 1		Camera 2		Fitness Functions	
Start point	End point	Start point	End point	$3DE$	C

$$C = \left|\frac{\partial u}{\partial x}\right|_{\min} + \left|\frac{\partial v}{\partial y}\right|_{\min} + \left|\frac{\partial w}{\partial z}\right|_{\min} \tag{6}$$

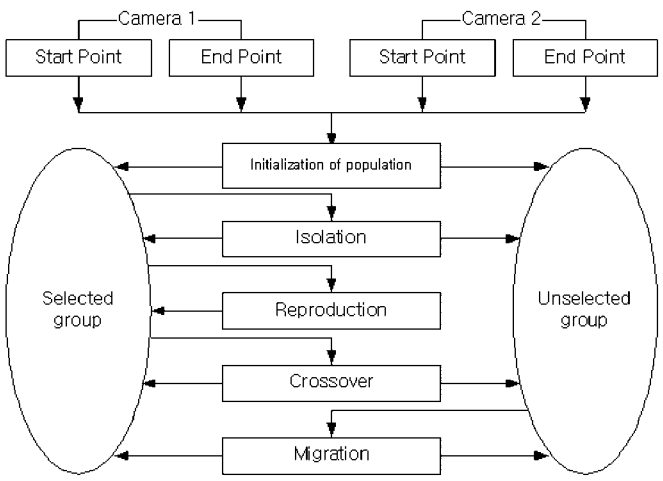

Fig. 2. Calculation procedure of GA-3D-PTV.

Equation (5) represents the mean value of the distance between the two points of a vector, i.e., the original point and the terminal point of a vector. D_o means the difference of the two three-dimensional positions of original vector points, (X_A, Y_A, Z_A) and (X_B, Y_B, Z_B). D_t means the difference of the two three-dimensional positions of vector terminal points, (X_A, Y_A, Z_A) and (X_B, Y_B, Z_B). After the initial population was determined, an isolation process was carried out using the threshold value $3DE$ again. The pairs of particles having a larger value than $3DE$ were isolated to the unselected group. Next, a reproduction process was made, where C value expressed as a fitness function as in Eq. (6) was used for refining the selected group. The reproduction process was followed by a cross-over process. In this process, the photographical data sets that can be regarded as two-dimensional vectors of each image of cameras were exchanged between the selected and unselected groups, and a separation of bad data sets from the unselected group was carried out by referencing the $3DE$ value again. In order to give a revival chance to the particles sorted into the inferior group (i.e. unselected group) up to now, a migration process was adapted. This process is similar to the initialization process. The above processes were repeated until paired particles were obtained. The threshold value $3DE$ was set to 0.5 mm and the crossover portion was 15% among the whole chromosomes generated. The three-dimensional velocity vectors were obtained by dividing the displacement of the paired particles with the time interval Dt, 1/60 sec.

2.3 Performance Test

Performance test for the proposed GA-3D-PTV algorithm was made by comparing the LES vector data sets proposed by Visualization Society of Japan (1999) with the vectors obtained by the proposed algorithm. Instantaneous vectors were randomly sampled by interpolating the LES data into space. The generation of virtual image was made using the selected vector data. Using the centroids of the virtual images of particles, three-dimensional vectors were calculated by the constructed algorithm. Okamoto et al. (1997) considered all possible parameters such as density of particle, image noises and etc. which construct a real experimental condition in generating virtual images. The generation procedures of the virtual images in this study are the same as the ones made by them.

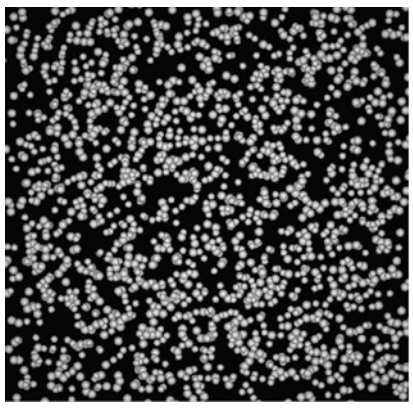

Fig. 3. Virtual image (N = 2000).

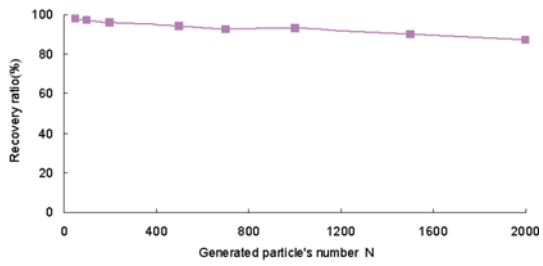

Fig. 4. Recovered vector ratio on an impinging jet.

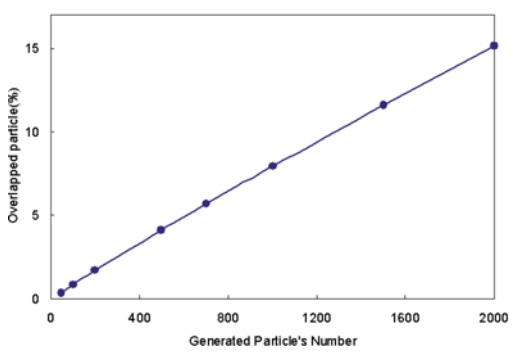

Fig. 5. Overlapped ratio among the generated particles.

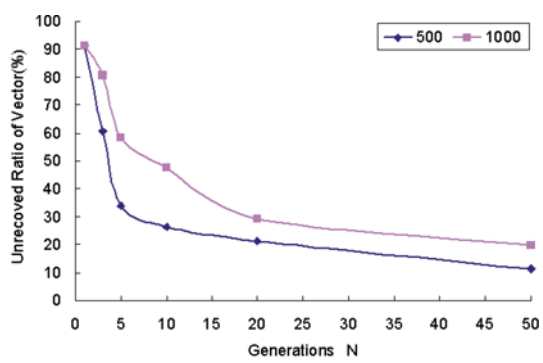

Fig. 6. Un-recovered vector ratio variation with generation N of GA calculation.

Figure 3 shows an example of the generated virtual images at the first instance. The images of the second instance were also generated by use of the LES data. Figure 4 shows a relationship between the number of particles used for the calculation of three-dimensional vector and the recovered vector numbers obtained by the constructed algorithm. The measured vectors of which magnitudes and coordinates had a slight difference within a threshold value with the reference vectors generated by the use of the LES data were regarded as correct vectors, i.e. recovered vectors. This curve shows the recovered vector number ratio with increases of particle numbers when the photographic coordinates of the particle centroids of the virtual images were used for the calculation of three-dimensional vectors. When the number of particle was 2000, the ratio of recovered correct vectors was about 80%. Figure 5 shows the ratio of the overlapped particles with increases of particle numbers. When the number of particles was 2000, the ratio of overlapped particles among the generated particles was about 15%. It is notable that this percentage is related with the remaining un-recovered vector ratio, 20%, as seen in Fig. 4 with the particle number, 2000. It was empirically verified in this study that most of original vectors were recovered without any error if there was no error in the coordinates of particles' centroids, which implies that most erroneous vectors were due to particles' overlapping which affects the accuracy of the particles' centroids. It was also empirically confirmed that the recovery ratio of the velocity vectors obtained in an actual experiment was slightly smaller than the results obtained in the performance test. Figure 6 shows the changes of the un-recovered vector ratio, erroneous vector ratio with respect to the number of particles, according to the change of the generation number N of the GA. One generation means that one calculation process is completed as shown in Fig. 2. With increase of the generation number the un-recovered vector ratio decreases up to the converged value, 20% when the number of particle was 2000. The calculation time for this case was about 4 minutes by the Pentium III (800 MHz) processor. The number of generation for the calculation of the present GA algorithm was about 70 for the case of particle number 2000.

2.4 Measurement Error Analysis

The measurement uncertainty was mainly caused by three elements, such as uncertainty in obtaining the three-dimensional positions of particles, uncertainty in obtaining the three-dimensional displacements of particles and uncertainty of the time interval between image frames. Generally, it is not so easy to analyze the uncertainty quantitatively in measuring the three-dimensional position error because of many parameters that affect the measurement error and also influence on each other non-linearly. In this study, the measurement uncertainty in measuring the three-dimensional position was evaluated by comparing the designed positional data of the landmark that were used for the actual experiment in the next section with the recovered positional data that were measured by the constructed system. Table 2 shows the standard deviation of the geometrical measurement errors, S_x, S_y and S_z. Since errors generated in obtaining velocity vectors are affected by the measurement errors of three-dimensional displacements and the errors of the time interval of image frames, the measurement uncertainty of velocity vectors was evaluated by considering these two factors. The measurement uncertainty of the displacement is caused by the errors of three-dimensional geometrical measurement. This uncertainty should be considered for both the starting and the terminal points of a vector. The error of the time interval was neglected. As a result, U_{RSS}, the measurement uncertainty of the displacement of a particle between consecutive images was estimated by Eq. (7) considering the uncertainty at the two points.

$$U_{\mathrm{RSS}} = [(2S_x)^2 + (2S_y)^2 + (2S_z)^2]^{1/2} \tag{7}$$

The value of U_{RSS} was about 0.14 mm between two image frames. The relative error of the measured velocity should be evaluated by considering this value. Figure 7 shows the changes of the relative error index S with the increase of particle numbers. The relative error index S was obtained by the following Eq. (8).

$$S = \frac{1}{M}\sum_{n}\frac{\left|V_{\mathrm{ref}} - V_{\mathrm{mea}}\right|}{V_{\mathrm{ref}}} \times 100\% \tag{8}$$

V_{ref} means the reference velocity vectors of the LES jet data mentioned in the previous section and V_{mea} means the measured velocity vectors by the constructed system. The notation n represents the number of the correct vectors. The error index increased with an increase of particle numbers. The error for v component was slightly higher than other components. The maximum relative error index reached up to about 3.5% at the number of particles of 2000. It was empirically verified that this error index could be reduced by the increase of camera resolutions.

Table 2. Errors of three-dimensional geometrical measurement.

Axis	X	Y	Z
Absolution mean value of errors [mm]	0.03	0.02	0.03
Standard deviation of errors [mm]	0.04	0.03	0.05

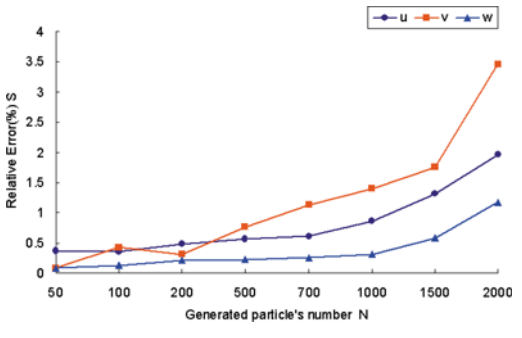

Fig. 7. Relative measurement error index S versus particle number N.

3. Measurements of the Wake of a Circular Cylinder

Figure 8 shows the overall arrangement for the measurement of the near wake of a cylinder (D = 10 mm) with the 3D-GA-PTV system. The measurement system consists of three cameras (768 × 494 pixels), an image grabber

(512 × 512 pixels, 8 bits) in the host computer (Pentium III) and an Ar-ion laser (500 mW). The three cameras were synchronized with AOM (Acousto-Optical Modulator) controller that was used to enhance the dynamic range of velocity measurement (Doh et al., 2000b) and they were installed nearly perpendicularly toward the measurement region so that the refraction at the wall of the experimental setup does not affect the measurement accuracy seriously. The cylinder was installed in a water channel (1200 × 300 × 300 mm) at the height of 100 mm from the bottom and 800 mm downstream from the flow stabilizer at upstream. The origin of the absolute coordinate (X = 0, Y = 0, Z = 0) was defined at the center of the cylinder as shown in Fig. 8. The measurement region in streamwise direction was between 0.1D and 5.0D from the origin of the absolute coordinate. The measurement volume was (X: 50 mm, Y: 50 mm, Z: 50 mm). The camera calibrator mentioned in the previous section was installed at the wake region of the cylinder to calculate the parameters of cameras. Nylon particles (d: 80 ㎛, s.g.: 1.02) were used as tracers. The particles were put into the water channel and illuminated by laser at the wake region of the cylinder. The maximum turbulent intensity of free-stream condition was about 0.8% and its distribution was uniform with the average value of 0.3% turbulent intensity at the inlet. Reynolds number and the water temperature were about 420 and 20°C, respectively.

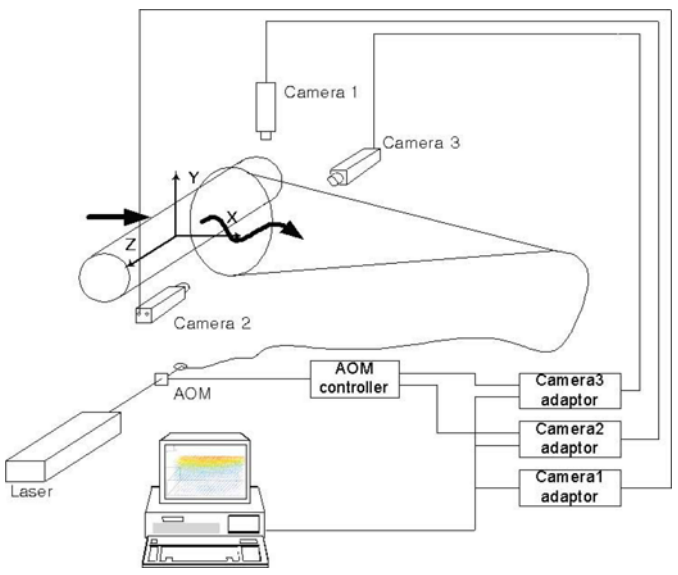

Fig. 8. GA-3D-PTV measurement system.

Figure 9 shows one of the images viewed by the camera 2. Figure 10 shows an instantaneous three-dimensional velocity vectors obtained in one processing. The number of instantaneous correct vectors was about 2000-3000. Figure 11 shows instantaneous vectors on a grid (11 × 13 × 12). Spatial and temporal interpolations

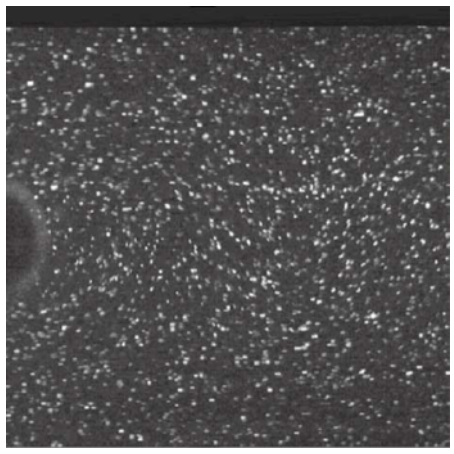

Fig. 9. Raw image viewed by camera 2.

were made to produce the grid vectors. A Gaussian window proposed by Agui and Jimenez (1987) has been used. The size of the window was 1.5 mm for spatial interpolation and 1/60 sec for temporal one. In order to obtain temporal properties of the flow field, 1200 consecutive image frames were utilized. The total number of instantaneous velocity vectors in obtaining several physical properties below was about 3000000.

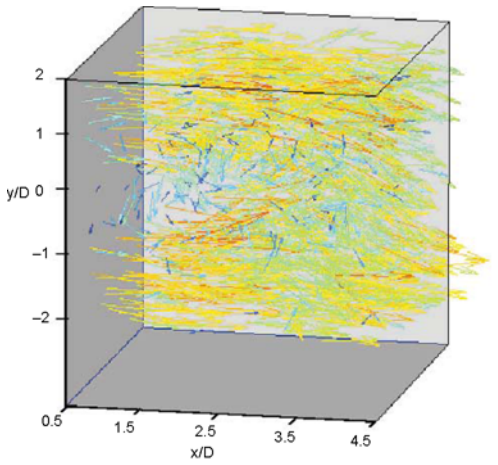

Fig. 10. Obtained instantaneous 3D velocity vectors.

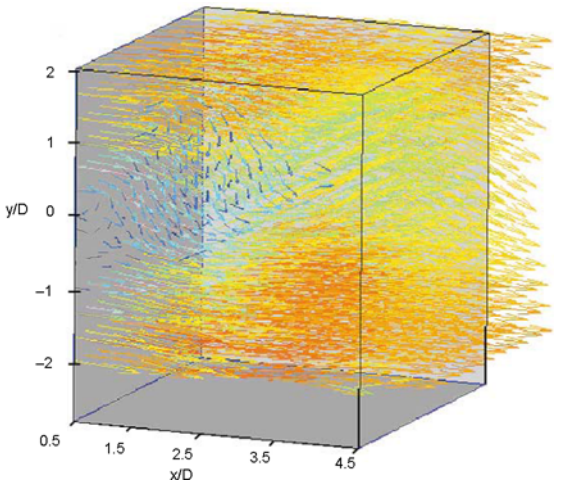

Fig. 11. Obtained instantaneous 3D velocity vectors on grids (11 × 13 × 12).

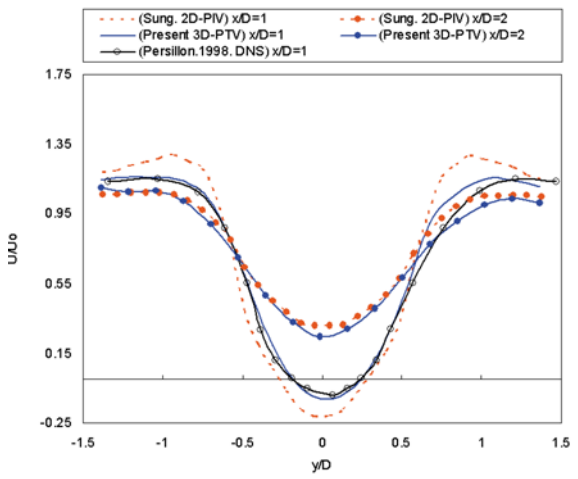

Fig. 12. Time mean velocity profile at x/D = 1.0.

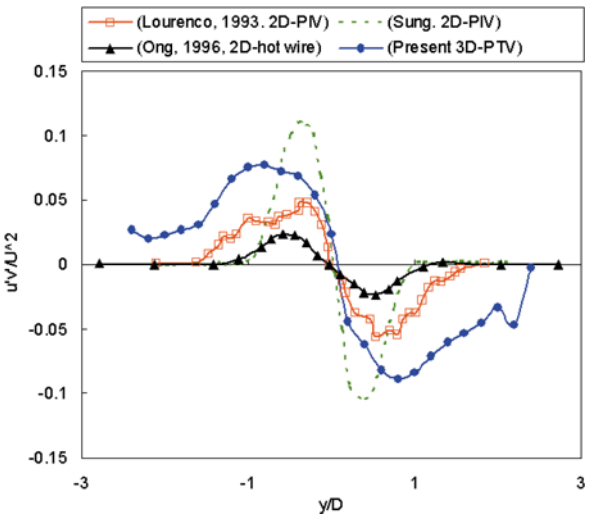

Fig. 13. Reynolds stress profile at x/D = 3.0.

Figure 12 shows the time mean velocity profile at x/D = 1.0. The measured values showed pretty good agreements with other results (Sung and Yoo, 2002; Persillon and Braza, 1998). Figure 13 shows the distribution of Reynolds stress, $u'v'/U_o^2$. Other results were based on two-dimensional PIV or hot wire methods. The qualitative results agree quite well with others. Since Sung and Yoo (2002) and Lourenco and Shih (1993) measured cylinder wake regions with Reynolds numbers 360 and 3900 respectively, it seems that the discrepancy with others is due to the differences in Reynolds numbers as well as experimental conditions such as inlet conditions. The streamwise time mean velocity profile along the centerline as shown in Fig. 14 was also similar to that of Lourenco and Shih (1993). Brede et al. (1996) proved that B-mode structures as shown in Fig. 15 are seen when the Reynolds number is higher than 300. The experimental results were supposed to show the B-mode structure, since the Reynolds number of the present case was 420.

Figure 16 shows instantaneous three-dimensional velocity vectors on three planes obtained by the constructed system. From these figures, it can be said that a structure like B-mode structures has been well reconstructed. The spanwise distance of the secondary vortices was about 1D as shown in the figures, which

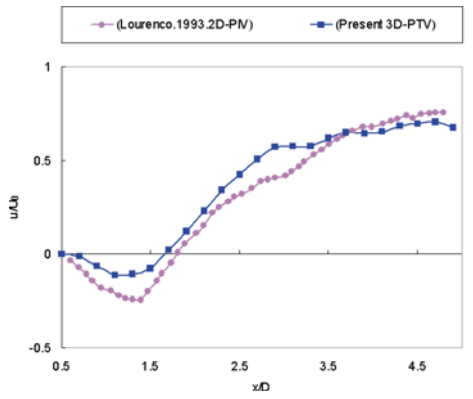

Fig. 14. Stream-wise time mean velocity profile along the centerline.

Fig. 15. B-mode vortices' structure (Brede et al., 1996).

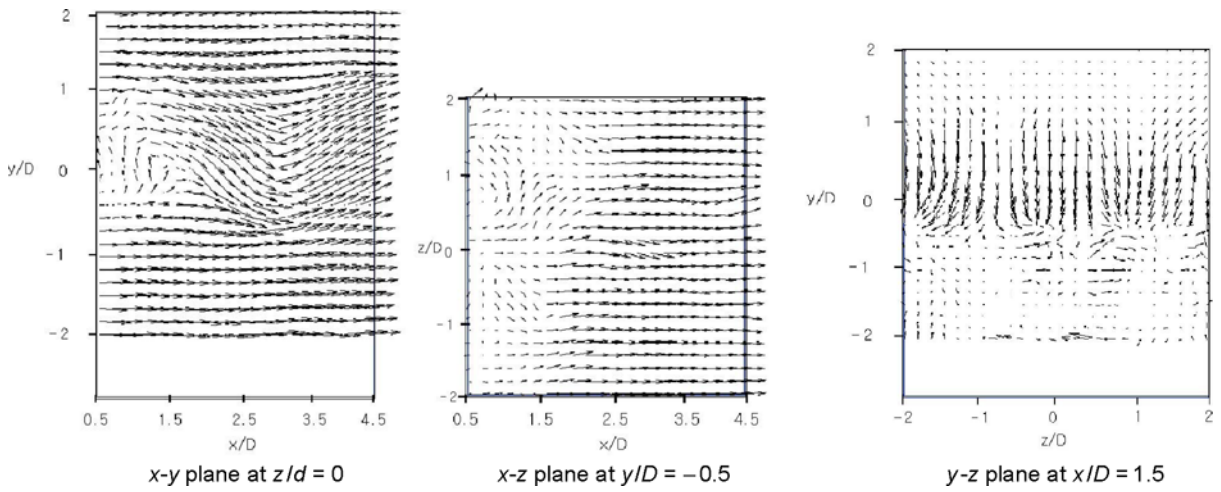

Fig. 16. Instantaneous 3D vectors on the planes.

agreed well with those reported by Wu et al. (1994) and Brede et al. (1996). Figure 17 shows the obtained normal Reynolds Stress of $w'w'/U_o^2$. Two peaks exist at $x/D = 1, 3$ but not at $x/D = 2$. This fact implies that there exists a characteristic streamwise distance $L = 2D$. Figure 18 shows a three-dimensional contour of instantaneous vorticity at a certain time. It seems that the shapes of the vorticity distribution along the spanwise direction of the cylinder are very similar to each other, which implies that spanwise structure is symmetric. The conspicuous streamwise

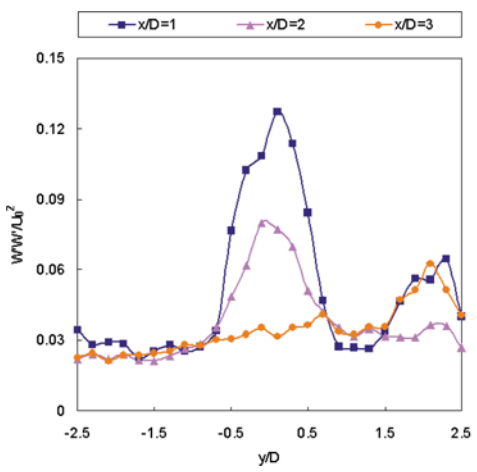

Fig. 17. Reynolds stress ($w'w'/U_o^2$) profile at different x/D.

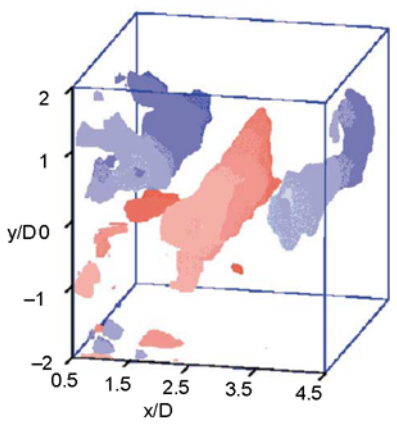

Fig. 18. 3D-contour of an instantaneous vorticity.

vortex structures are regularly convected downward rolling up and down and the distance between them is about 2*D*. This distance can be regarded as the characteristic length as explained for the case of Fig. 17. Figure 19 shows an instantaneous spatial distribution of turbulent kinetic energy $q^2 = 1/2(\overline{u'^2} + \overline{v'^2} + \overline{w'^2})$. The vortices shed from the upper and lower edges of the cylinder generate the turbulent kinetic energies and these energies were merged at the position of x/D = 2.5 and then were convected downward without any mixing. It was found that the distribution of the turbulent kinetic energy was uniform along the spanwise direction and the positions showing the highest turbulent kinetic energy existed between the stream vortex structures as shown in Fig. 19. It can be figured out from Figs. 18 and 19 that the B-mode vortex structures obviously exist regularly along the spanwise and the streamwise directions. This fact strongly supports that the constructed 3D-PTV system can measure instantaneous vortex structures of the cylinder wake.

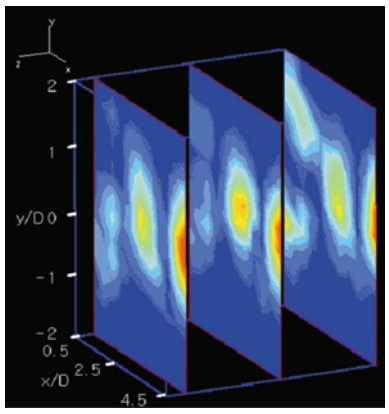

Fig. 19. Instantaneous *RMS* turbulent kinetic energy distribution.

4. Conclusions

A new 3D-PTV technique using a genetic algorithm (GA) has been developed and its application to the measurement of the near wake of a circular cylinder has successfully been made. Conclusions obtained during the construction process of the new GA-3D-PTV system can be summarized as following.

A new GA based 3D-PTV was constructed using non-metric three CCD cameras. The performance test of the constructed system has been carried out by using the sets of virtual images generated by an LES data set on a jet flow. It was verified that the correct vector recovery ratio was fairly good enough to probe the structures of complex flows and the recovery ratio was strongly dependent upon the overlapping of particles.

In the actual measurement, about 2000-3000 instantaneous three-dimensional velocity vectors could be obtained from about 3000-4000 particles. This implies that the recovery ratio was larger than about 75% in the actual experiment. This percentage is the highest compared with other existing three-dimensional PTV techniques. The fact that the results have been achieved by the cameras of only 512 × 512 pixel resolutions implies the possibility of direct probing of any complex flows if high-definition cameras and video systems are provided.

A performance test using LES data showed that the relative measurement error was less than 5%.

Comparison of the measured data with others showed quite reasonable agreement. Several physical properties, such as time mean and instantaneous velocity profiles, three-dimensional distribution of turbulent kinetic energy, spatial distribution of vortices and others were successfully measured with the constructed system. Other physical properties were also able to be composed through the turbulent kinetic energy.

B-mode structures (Brede et al., 1996) were clearly captured by the constructed GA-3D-PTV system. The results obtained by the system showed good qualitative and quantitative agreements with others. The constructed system can be used for the investigation of the turbulent properties of complex flows up to micro scales if the limitations of the constructed system, such as resolution and image noise problem, are overcome.

Acknowledgments

This work was supported by grant No. 2001-1-300400-001-1 (R05-2001-000-01066-0) from the Basic Research Program of the Korea Science & Engineering Foundation.

References

Adrian, R. J., Particle-Imaging Techniques for Experimental Fluid Mechanics, Ann. Rev. Fluid Mech., 23 (1991), 261.

Agui, J. C. and Jimenez, J., On the Performance of Particle Tracking, J. Fluid Mech., 185 (1987), 447.

Ballard, D. H. and Brown, C. M., Computer Vision, (1982), 195, Prentice-Hall, New Jersey.

Brede, M., Eckelmann, H. and Rockwell, D., On Secondary Vortices in the Cylinder Wake, Phys. Fluids, 8 (1996), 2117-2124.

Chang, T. P. and Tatterson, G. B., An Automated Analysis Method for Complex Three Dimensional Mean Flow Fields, Proc. Third Int. Symp. Flow Visualization (1983), 266-273.

Doh, D. H., A Study on Three Dimensional Particle Imaging Thermometry and Velocimetry Using Liquid Crystal, Ph.D. Thesis, The Univ. of Tokyo (1995).

Doh, D. H., Cho, K. R., Baek, T. S. and Cho, Y. B., 3D-PTV Using a Genetic Algorithm, Proc. of Winter Annual Conference, the Society of Air-conditioning and Refrigeration Engineers of Korea, Vol. 2 (2000a), 601-605.

Doh, D. H., Kim, D. H., Choi, S. H., Hong, S. D., Saga, T. and Kobayashi, T., Single-Frame (Two-Field Image) 3D-PTV for High Speed Flows, Exp. in Fluid, Suppl. (2000b), 85-98.

Goldberg, D. E., Optimal Initial Population Size for Binary-coded Genetic Algorithm, TCGA Report No. 85001, Univ. of Alabama (1985).

Kasagi, N., Hirata, M., Nishino, K., Ninomiya, N. and Koizumi, N., Three-dimensional Velocity Measurement via Digital Image Processing Technique, J. of Flow Visualization Soc. Jpn., 7-26 (1987), 283-288.

Kasagi, N. and Nishino, K., Probing Turbulence with Three Dimensional Particle Tracking Velocimetry, Exp. Thermal and Fluid Sci. 4 (1991), 601-612.

Kobayashi, T., Saga, T. and Sekimoto, K., Velocity Measurement of Three-dimensional Flow Around Rotating Parallel Disks by Digital Image Processing, ASME FED, No. 85 (1989), 29-36.

Kobayashi, T., Saga, T., Haeno, T. and Tsuda, N., Development of a Real-time Velocity Measurement System for High Reynolds Fluid Flow Using a Digital Image Processing Design, Experimental and Numerical Flow Visualization (Ed. Khalighia, B. et al.), ASME FED, No. 128 (1991), 9-14.

Lourenco, L. M. and Shih, C., Characteristics of the Plane Turbulent Near Wake of a Circular Cylinder, A Particle Image Velocimetry Study (1993), (extracted from Mittal (1996)).

Maas, H. G., Gruen, A. and Papantoniou, D. A., Particle Tracking Velocimetry in Three-dimensional Flows, Part 1 Photogrammetric Determination of Particle Coordinates, Exp. in Fluids, 15 (1993), 133-146.

Mittal, R., Progress on LES of Flow Past a Circular Cylinder, Annual Research Briefs-1996, Center for Turbulence Research, Stanford Univ. NASA Ames Research (1996), 233-241.

Ohyama, R., Takagi, T., Tsukiji, T., Nakanishi, S. and Kaneko, K., Particle Tracking Technique and Velocity Measurement of Visualized Flow Fields by means of Genetic Algorithms, J. of Flow Visualization Soc. Jpn., 13-Suppl. No. 1 (1993), 22-25.

Okamoto, K., Nishio, S., Kobayashi, T. and Saga, T., Standard Images for Particle Imaging Velocimetry, Proc. PIV'97-Fukui (Fukui), (1997), 229-236.

Ong, L. and Wallace, J., The Velocity Field of the Turbulent Very Near Wake of a Circular Cylinder, Exp. in Fluids, 20 (1996), 441-453.

Persillon, H. and Braza, M., Physical Analysis of the Transition to Turbulence in the Wake of a Circular Cylinder by Three-dimensional N-S Simulation, J. Fluid Mech., 365 (1998), 23-88.

Racca, R. G. and Dewey, J. M., A Method for Automatic Particle Tracking in a Three-dimensional Flow Field, Exp. in Fluids, 6 (1988), 25-32.

Sung, J. and Yoo, J. Y., Near-Wake Vortex Motions Behind a Circular Cylinder at Low Reynolds Number, Journal of Fluids and Structures, to be published (2002).

Utami, T. and Blackwelder, R., A Cross Correlation Technique for Velocity Field Extraction from Particulate Visualization, Exp. in Fluids, 10 (1991), 213-223.

Visualization Society of Japan, Standard Project, Visualization Society of Japan (1999), http://vsj.or.jp/piv

Wu, J., Sheridan, J., Welsh, M. C., Hourigan, K. and Thompson M., Longitudinal Vortex Structures in a Cylinder Wake, Phys. Fluids, 6 (1994), 2883-2885.

Yamada, H. and Yamane, K., Particle Image Velocimetry Using a Genetic Algorithm, J. of Flow Visualization Soc. Jpn., 15-Suppl. No.1 (1995), 165-168.

Author Profile

Deog Hee Doh: He received a B.A. at Korea Maritime University (1985). He finished his M.S. degree at the Graduate School of Korea Maritime University (1988). He received his Ph.D. degree at the Department of Mechanical Engineering of the University of Tokyo, Japan in 1995. His graduate work was issuing the development of 3D-PTV and simultaneous measurement techniques on temperature and velocity fields for thermal turbulent flows. He worked as an invited researcher for the Advanced Fluid Engineering Research Center (AFERC) in 1995. He has been working for Korea Maritime University since 1995 at the School of Mechanical and Information Engineering. His major research interest is to develop spatial measurement techniques such as 3D-PIVs, 3D-PTVs for the analysis of turbulent flows, and VR (Virtual Reality).

Dong Hyuk Kim: He received his B.S. (Eng.) degree in Mechanical Engineering in 1976 from Seoul National University, M.S. (Eng.) from New Jersey Institute of Technology and Ph.D. in Mechanical Engineering in 1988 from the Johns Hopkins University. He worked at the Agency for Defense Development in Korea before his graduate study. After obtaining his Ph.D. he had worked as a senior researcher at the Korea Standard Research Institute until 1992. Now he is a professor in the division of Mechanical and Informational Engineering at Korea Maritime University. His research interest covers multiphase flow including bubble dynamics, thermoacoustics and PIV measurement systems.

Kyung Rae Cho: He was educated at Korea Maritime University (B.A. 1998). He received M.S. degree at Korea Maritime University. His research interest covers 3D-PIVs, 3D-PTVs and Turbulences.

Yong Bum Cho: He is currently pursuing a M.S. Degree from Department of Mechanical Engineering of Korea Maritime University. His research interest is fluid dynamics using 3D-PIVs and 3D-PTVs methods.

Won Je Lee : He is currently pursuing a M.S. Degree from Department of Air-Conditioning & Refrigeration Engineering of Korea Maritime University. His research interest is fluid dynamics using 3D-PIVs and 3D-PTVs methods.

Tetsuo Saga: He graduated from Japan University in 1966 and he is a research associate in the Institute of Industrial Science, the University of Tokyo. His main research field is mechanical engineering. His research interests include flow visualization and its image analysis, prediction and control of flow induced vibration and automobile aerodynamics. Recently, he has interests in micro flow and bio flow analysis using PIV.

Toshio Kobayashi: He received his Ph.D. in the Mechanical Engineering Department, at the University of Tokyo in 1970. After completion of his Ph.D. program, he has been a faculty member of the Institute of Industrial Science (IIS), the University of Tokyo, and currently is a professor. His research interests are numerical analysis of turbulence, especially Large Eddy Simulation and Particle Image Velocimetry. He serves as the President of the Visualization Society of Japan (VSJ), Executive Vice President of Automotive Engineers of Japan (JSAE) and President of the Japan Society of Mechanical Engineers (JSME).